Rare Met. (2018) 37(8):675–681
https://doi.org/10.1007/s12598-016-0837-x

RARE METALS
www.editorialmanager.com/rmet

Microstructure and properties of MOCVD-derived $Gd_xY_{1-x}Ba_2Cu_3O_{7-\delta}$ films with composition fluctuations

Yu-Xi Zhang, Fei Zhang, Rui-Peng Zhao, Yan Xue, Hui Wang, Qiu-Liang Wang, Jie Xiong*, Bo-Wan Tao

Received: 15 November 2015 / Revised: 23 November 2015 / Accepted: 4 December 2016 / Published online: 23 February 2017

Abstract The effects of Gd content on crystalline orientation, microstructure and superconductivity of $Gd_xY_{1-x}Ba_2Cu_3O_{7-\delta}$ (GdYBCO) films were systematically investigated. By varying the Gd content in the liquid precursor without changing the total amount of rare earth elements, series of GdYBCO films with x values of 0, 0.1, 0.3, 0.5, 0.7, 0.9 and 1.0 were fabricated by metal organic chemical vapor deposition (MOCVD). X-ray diffraction (XRD) and scanning electron microscope (SEM) analysis revealed that Gd introducing could restrain the formation of $CuYO_2$ phase, but induce a-axis growth of GdYBCO film. The increase of x from 0 to 0.5 leads to enhancing critical current density at self-field and 77 K (J_{csf}) from 1.8 to 2.8 MA·cm^{-2}, which benefits from the decrease in $CuYO_2$ impurities and improvement of in-plane texture from 5.0° to 4.3°. However, raising x from 0.5 to 1.0 gives rise to abundant a-axis growth of film and degradation of in-plane texture from 4.3° to 5.4°, consequently resulting in the decrease of J_{csf} from 2.8 to 0.8 MA·cm^{-2}. Even though J_{csf} has not varied monotonically, the critical transition temperature of GdYBCO films linearly increases from 90.75 to 92.25 K and the in-field performance at magnetic field (B) of 0–1.1 T and 77 K as well as B parallel to film normal is also superior with Gd content increasing.

Y.-X. Zhang, F. Zhang, R.-P. Zhao, Y. Xue, J. Xiong*, B.-W. Tao
State Key Laboratory of Electronic Thin Film and Integrated Devices, University of Electronic Science and Technology of China, Chengdu 610054, China
e-mail: jiexiong@uestc.edu.cn

H. Wang, Q.-L. Wang
Applied Research Laboratory of Superconduction and New Material, Institute of Electrical Engineering, Chinese Academy of Sciences, Beijing 100190, China

Keywords Gd content; GdYBCO; MOCVD; Microstructure; Flux pinning

1 Introduction

Critical current density (J_c) of $YBa_2Cu_3O_{7-\delta}$ (YBCO) superconducting film decays severely with applied magnetic field due to the motion of vortices [1]. How to immobilize the vortices to improve the in-field performance of YBCO film has captured the researchers' attention. Although naturally grown defects [1], such as boundaries, in-plane or out-of-plane misorientation, dislocations and voids, can somewhat pin flux vortices, yet reports [2–6] have revealed that the density or effectiveness of these naturally grown defects was not high enough to retain high-field J_c at a necessary level.

Substantial efforts on introducing artificial pinning centers (APCs) have been made to improve the flux pinning effects. For instance, nano-sized Y_2O_3 particles resulted from the excess of yttrium in YBCO films could form point, line and/or plane defects, thus enhanced the flux pinning effects [7–10]. Alternatively, perovskites such as $BaZrO_3$ [10–15], $BaSnO_3$ [16], $BaHfO_3$ [17] and $BaIrO_3$ [18] could also form randomly oriented particles or c-axis oriented columnar defects in YBCO matrix to improve the flux pinning effects. Additionally, inclusion of nanoparticles of Gd_3TaO_7 [19], Ba_2GdTaO_6 [20], Ba_2YNbO_6 [21], YBa_2CuO_5 [22] or Y_2BaCuO_5 [23] has also been demonstrated to be an effective way to raise the in-field performance of YBCO films. In addition to introduction of the above-mentioned extra particulates, the partial or complete substitution of lanthanides for yttrium to form REBCO (RE = rare earth) has also manifested the enhanced flux pinning effects. As an example, $GdBa_2Cu_3O_{7-\delta}$ (GdBCO)

was reported being of superior in-field performance to YBCO [24]. However, systematic research about the effects of Gd content on the properties of $Gd_xY_{1-x}Ba_2Cu_3O_{7-\delta}$ (GdYBCO) superconducting films has been barely reported [25].

Hence, the authors have applied metal organic chemical vapor deposition (MOCVD) to fabricate GdYBCO films with various Gd contents on the metallic substrates and systematically investigated the effects of Gd content on the crystalline orientation, in-plane and out-of-plane textures, surface morphology, self-field and in-field superconductivity at 77 K.

2 Experimental

The MOCVD system applying single mixed liquid precursor of metal organics was used to deposit GdYBCO films. And the home-made buffer stack of $LaMnO_3$/homo-epi MgO/ion beam-assisted deposition (IBAD)-MgO/Y_2O_3/Al_2O_3/Hastelloy tape [26, 27], collectively termed as IBAD template, was used as substrate, which was preheated to 810 °C during the deposition of GdYBCO film. The precursor was prepared by dissolving solid-state metal organics of $Y(tmhd)_3$, $Gd(tmhd)_3$, $Ba(tmhd)_2$ and $Cu(tmhd)_2$ into tetrahydrofuran. To fabricate GdYBCO films with various Gd contents, the mole ratio of Gd to the constant total amount of Gd and Y in precursor was set as 0%, 10%, 30%, 50%, 70%, 90% and 100%, corresponding to x values of 0, 0.1, 0.3, 0.5, 0.7, 0.9 and 1.0 in GdYBCO film, respectively. More experimental details could be found elsewhere [28].

The crystalline orientation and texture of as-deposited GdYBCO films were examined by X-ray diffractometer (XRD, Bede D1). The microstructure was observed by scanning electron microscope (SEM, JEOL JSM-7001F). The critical transition temperature (T_c) was measured by four-probe method using the current of 1 mA, and the GdYBCO samples were cooled by cold head of Sumitomo (RDK-101D). The J_c at 77 K and 0 T (J_{csf}) was obtained by induction method using Leipzig J_c-scan system. The critical current in the magnetic field (B) from 0 to 1.1 T was measured on the sample bridge of 1 mm × 5 mm (width × length) with magnetic field direction parallel to the film normal, and the criteria to determine the critical current was 1 $\mu V \cdot cm^{-1}$. Additionally, the film thickness was tested by step profiler (Veeco, Dektak 150).

3 Results and discussion

500-nm-thick GdYBCO films with x values of 0, 0.1, 0.3, 0.5, 0.7, 0.9 and 1.0 were fabricated on IBAD-MgO templates. Figure 1 shows the detailed θ–2θ patterns, which exhibit clear and sharp peaks of (00l) GdYBCO and a few unexpected peaks of $CuYO_2$ phases and (h00) GdYBCO. As $x < 0.5$, only (00l) GdYBCO peaks can be clearly observed, indicating that the corresponding films crystallize well and align their c-axis perpendicular to the substrate surface. However, the films mix with a few $CuYO_2$ particles, demonstrated by the presence of $CuYO_2$ peaks in Fig. 1. As $x \geq 0.5$, the peaks of $CuYO_2$ disappear, revealing that the increase in Gd content prevents the formation of $CuYO_2$ precipitates and the composition ratio of the film body is closer to the stoichiometric value. However, the presence of (h00) GdYBCO peaks suggests that the film transfers from purely c-axis orientation to mixed orientation of c-axis and a-axis. It should also be noted that the intensity of (002) peak of the film becomes weaken with Gd content increasing. To give quantitative understanding, $I_{(002)}$ and $I_{(003)}$ are used to represent the intensities of (002) peak and (003) peak of the film, respectively, and the $I_{(003)}/I_{(002)}$ values are summarized in Fig. 2. It is obvious that $I_{(003)}/I_{(002)}$ value is enlarged as Gd content increases. As reported in Ref. [29], it is the intrinsic character of GdBCO that the (002) peak is much weaker than (003) peak. Hence, it is easy to understand that such increase in $I_{(003)}/I_{(002)}$ ratio is ascribed to the change of film body from YBCO to GdBCO with Gd content increasing from 0 to 1. Conversely, the curve in Fig. 2 can also be used to semi-quantitatively determine the Gd content of GdYBCO film when the Gd content is uncertain.

Figure 3 shows χ-scans [30] on (102) planes of all GdYBCO films. As $x < 0.5$, there is only one peak around 57° corresponding to (102) plane of c-axis oriented GdYBCO grains, whereas there arises one more peak around 33° corresponding to (102) planes of a-axis oriented GdYBCO grains when x further increases to 1.0. The

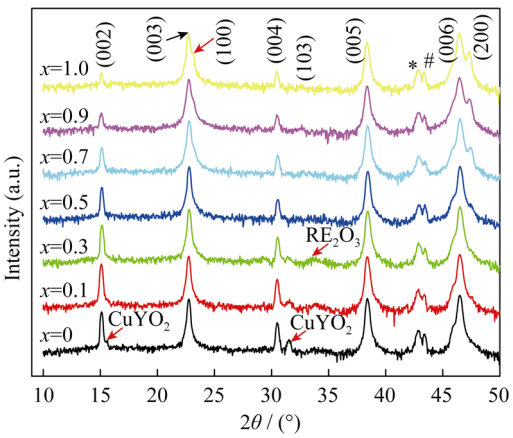

Fig. 1 XRD θ–2θ patterns of GdYBCO films fabricated at various Gd contents (x value). Symbols asterisk and number sign indicating diffraction peaks of MgO and Hastelloy tape, respectively

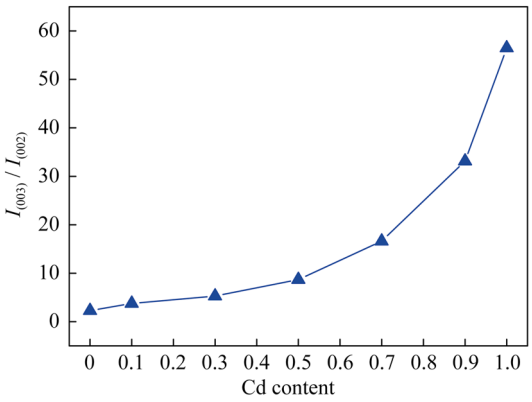

Fig. 2 Relationship between ratio value of $I_{(003)}/I_{(002)}$ and Gd content. $I_{(003)}$ and $I_{(002)}$ representing peak intensities of (003)GdYBCO and (002)GdYBCO, respectively

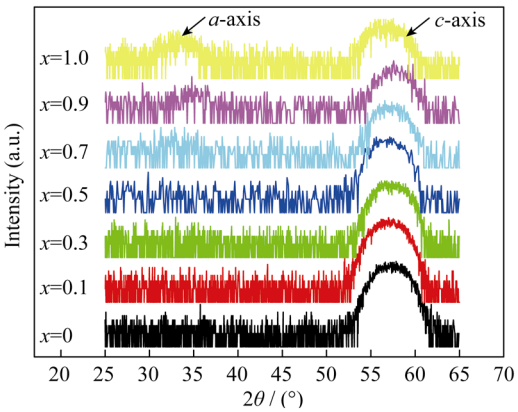

Fig. 3 XRD χ-scans of (102)GdYBCO of as-fabricated films

above-obtained results are in agreement with those yielded from 2θ scans, further demonstrating that the orientation of GdYBCO films transfer from *c*-axis orientation to *a*-axis orientation. Such conversion of orientation suggests that the MOCVD conditions optimized for YBCO film deposition are not appropriate any more, since the film body has transferred from YBCO to GdBCO as $x > 0.5$. For example, with experiments it has been found that the deposition temperature of GdBCO film was about 15 °C higher than that of YBCO film.

To determine the out-of-plane and in-plane textures of the films, the ω-scans and Φ-scans were performed, respectively, on (005) GdYBCO and (103) GdYBCO, and the corresponding full width at half maximum (FWHM) values ($\Delta\omega$, $\Delta\Phi$) are summarized in Fig. 4. As Gd content rises up to 0.5, $\Delta\omega$ hardly changes, while $\Delta\Phi$ decreases from 5.0° to 4.3°, indicating that Gd substitution for Y deeply improves the in-plane texture rather than out-of-plane texture. Such improvement on in-plane texture would be owed to the disappearance of $CuYO_2$ impurities. However, $\Delta\Phi$ is enlarged as Gd content further increases, suggesting that the in-plane texture deteriorates. And this

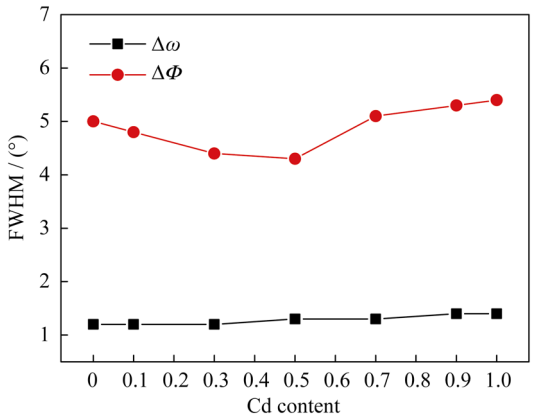

Fig. 4 Relationship of FWHMs of ω-scans on (005) planes and Φ-scans on (103) planes of GdYBCO films with various Gd contents

deterioration is attributed to the appearance of *a*-axis oriented growth, which results from the above-mentioned improper deposition conditions of GdYBCO films.

SEM images of GdYBCO films are shown in Fig. 5, exhibiting dense and crack-free microstructure as well as some surface particles. As $x = 0$, there is a large number of particles identified as Y–Cu–O phases by energy dispersive spectroscopy (EDS) analysis (not shown here), which is consistent with the XRD examinations in Fig. 1. As x is enlarged, the number of Y–Cu–O particle decreases, which is in agreement with the weakening of diffraction peak of $CuYO_2$ phase in Fig. 1. However, the *a*-axis oriented GdYBCO grains (rectangular shape particles in Fig. 5) also arise with Gd content increasing, especially for $x > 0.5$. When $x > 0.5$, the size and density of *a*-axis grains increase with Gd content increasing, consistent with the higher (*h*00) GdYBCO peaks at larger x in Fig. 1. Such microstructure with large number of *a*-axis grains for $x > 0.5$ further demonstrates that the deposition conditions are not appropriate anymore and the substrate temperature is somewhat low, especially for those of higher Gd content.

The superconductivity of GdYBCO film is characterized by the measurements of critical transition temperature (T_c) and J_{csf}, of which the results are depicted in Fig. 6. In Fig. 6a, the T_c almost linearly increases from 90.75 to 92.25 K, whereas the transition width (ΔT) firstly increases and then decreases with the increase in Gd content. And ΔT is 0.65 and 0.93 K for YBCO and GdBCO, respectively, and reaches its maximum of $\sim$2 K at $x = 0.5$. Owing to the higher T_c of GdBCO than YBCO, such variation of ΔT results from the co-existence of YBCO phase and GdBCO phase at $0 < x < 1.0$. In Fig. 6b, J_{csf} increases from 1.8 to 2.8 MA·cm^{-2} as $0 \le x \le 0.5$, which benefits from the rising of T_c and the above-mentioned improvement of in-plane texture yielded from the decrease in $CuYO_2$ impurities. When Gd content is above 0.5, the film body transfers to GdBCO and the improper deposition

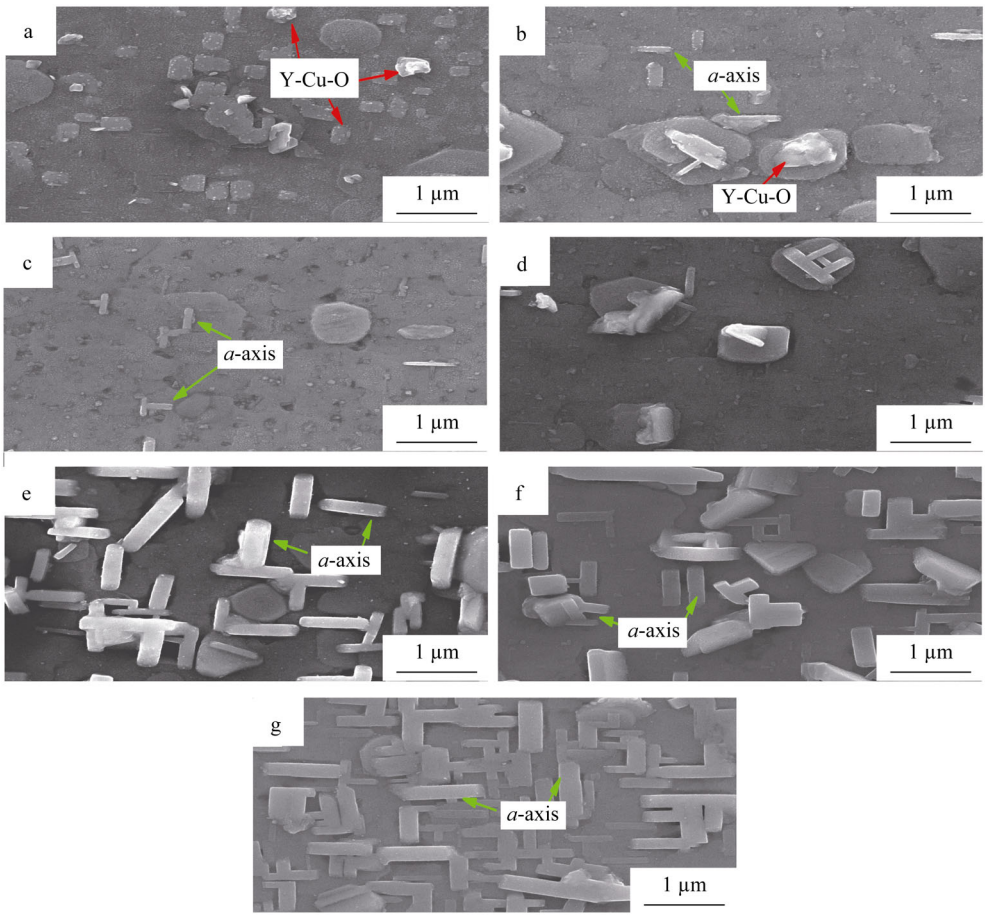

Fig. 5 SEM images of GdYBCO films with various Gd contents: **a** $x = 0$, **b** $x = 0.1$, **c** $x = 0.3$, **d** $x = 0.5$, **e** $x = 0.7$, **f** $x = 0.9$ and **g** $x = 1.0$

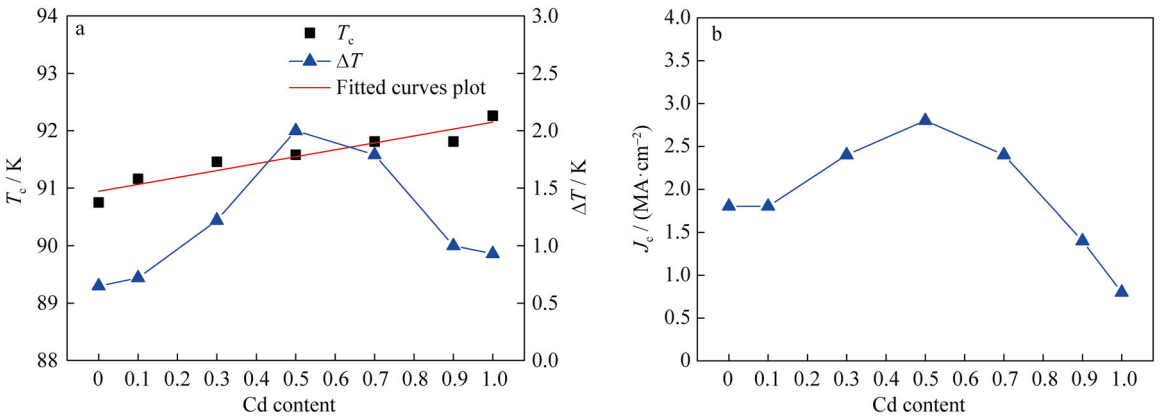

Fig. 6 Dependence of superconductivity of as-deposited GdYBCO films on Gd content: **a** critical transition temperature (T_c) and transition width (ΔT) and **b** J_c at 77 K and 0 T

conditions leads to the degradation of in-plane and out-of-plane textures as well as the presence of misoriented grains including (103) GdYBCO and (*h*00) GdYBCO. The texture degradation and grain misorientation are harmful to the transmission of superconducting current, consequently resulting in the drop of J_{csf} from 2.8 to 0.8 MA·cm^{-2}.

The dependence of critical current (I_c) on B was measured on the samples with Gd content of 0, 0.3, 0.5, 0.7 and 1.0 at 77 K and plotted in Fig. 7a, which shows that I_c of all samples declines with B. To intuitively exhibit the effects of Gd content, the curves in Fig. 7a are normalized by $I_c(B = 0)$ and replotted in Fig. 7b. It is clearly

illustrated that the increase in Gd content slows down the declining rate of normalized $I_c/I_c(B = 0)$ with B increasing, which benefits from the flux pinning effects induced by substituting Gd for Y [24, 25]. At $B = 1$ T and 77 K, the normalized $I_c/I_c(B = 0)$ corresponding to Gd content of 1.0 retains about 27%, twice more than that of Gd content of 0, demonstrating that GdBCO film has in-field performance quite superior to that of YBCO film at 77 K. As reported, $I_c(B)$ is proportional to $B^{-\alpha}$ in the field range of 0.1–1.0 T (α value is calculated from the I_c–B curve in Fig. 7) and the smaller α value means the better in-field performance [1]. By fitting the data points (shown in inset of Fig. 7b), the α values corresponding to Gd content of 0, 0.3, 0.5, 0.7 and 1.0 are 0.400, 0.397, 0.394, 0.375 and 0.332, respectively, among which the smallest value of 0.332 is comparable to those reported α values [12, 13, 15, 31]. Figure 8 shows the magnetic field dependence of flux pinning force (F_p), where $F_p = J_c(B) \times B$ [31]. And $J_c(B)$ is deduced from the data in Fig. 7a through the following equation:

$$J_c(B) = \frac{I_c(B)}{w \times t} \quad (1)$$

where w and t represent the width and thickness of the micro-bridge of GdYBCO films used in I_c measurements, being 1 and 500 nm, respectively.

In view of the various J_{csf} shown in Fig. 6b, the comparative analysis of Gd content of 0 and 1.0 as well as 0.3 and 0.7 is more illustrative. With regard to Gd content of 0 and 1.0, F_p of the former is higher than that of the latter as $B < 0.2$ T, which is attributed to the much higher J_{csf} of 1.8 MA·cm^{-2} of the former than 0.8 MA·cm^{-2} of the latter. As 0.2 T $< B <$ 1.0 T, F_p of Gd content of 1.0 is almost same with that of Gd content of 0, indicating that the flux pinning effect of GdBCO is stronger than that of YBCO at this moment. As for Gd content of 0.3 and 0.7, they have the same J_{csf} and their F_p is same too as $B < 10$ mT, whereas F_p of the latter is increasingly higher

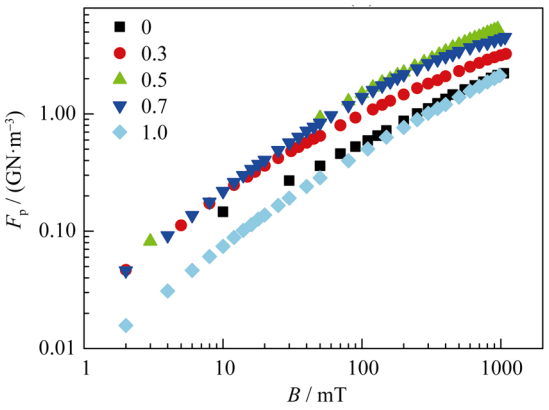

Fig. 8 Magnetic field (B) dependence of flux pinning force (F_p), where $F_p = J_c \times B$

than that of the former as B increases to 1.0 T, suggesting that the latter is of superior flux pinning effect. All the above discussion suggests that substitution of Gd for Y is beneficial to enhance the flux pinning effect of the film.

4 Conclusion

Gd content deeply affects the in-plane texture, morphology and superconducting performance of GdYBCO films. The increase in Gd content from 0 to 0.5 could suppress the formation of $CuYO_2$, thus improves the in-plane texture and microstructure of the films and finally enlarges J_{csf} from 1.8 to 2.8 MA·cm^{-2}. As Gd content further increases from 0.5 to 1.0, the growth of a-axis GdYBCO grains arises abundantly and becomes much severer at Gd content of 1.0, which consequently deteriorates the texture and thus drops J_{csf} from 2.8 to 0.8 MA·cm^{-2}. However, the increasing Gd content brings the linear increase of T_c from 90.75 to 92.25 K and the slower decay of normalized $I_c/I_c(B = 0)$ as well as the stronger flux pinning effect. Even though the flux pinning

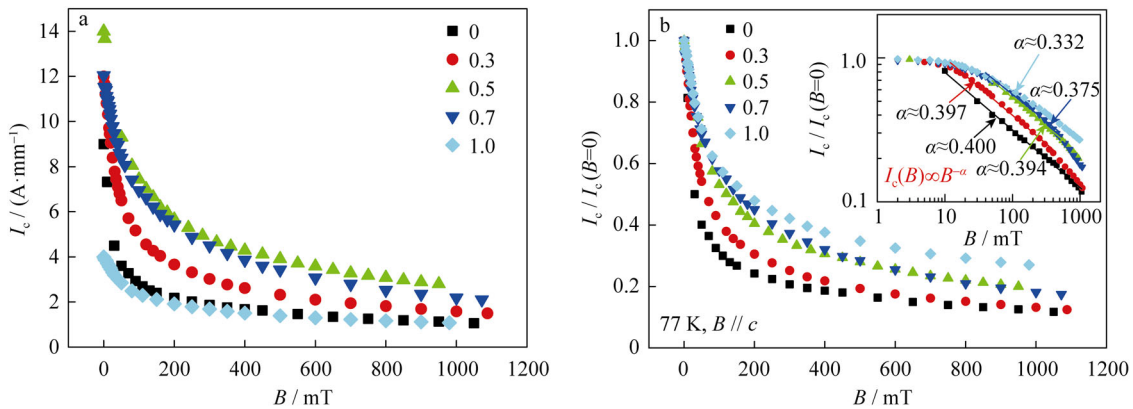

Fig. 7 Dependence of **a** critical current (I_c) and **b** normalized I_c/I_c ($B = 0$) on magnetic field (B) with B perpendicular to normal of sample surface

force of GdBCO is smallest due to the lowest J_c, the authors believe that further modification on MOCVD process would raise J_c and then enhance the flux pinning force.

Acknowledgements This study was financially supported by the National Science Foundation of China (No. 91421110), the National High Technology Research and Development Program of China (No. 2014AA032702), the National Basic Research Program of China (No. 2015CB358600), the Sichuan Youth Science and Technology Innovation Research Team Funding (No. 2011JTD0006) and the Sichuan Provincial Fund for Distinguished Young Academic and Technology Leaders (No. 2014JQ0011).

References

[1] Foltyn SR, Civale L, MacManus-Driscoll JL, Jia QX, Maiorov B, Wang H, Maley M. Materials science challenges for high-temperature superconducting wire. Nat Mater. 2007;6(9):631.

[2] Hylton TL, Beasley MR. Flux-pinning mechanisms in thin films of $YBa_2Cu_3O_{7-\delta}$. Phys Rev B. 1990;41(16):11669.

[3] Blatter G, Feigelman MV, Geshkenbein VB, Larkin AI, Vinokur VM. Vortices in high temperature superconductors. Rev Mod Phys. 1994;66(4):1125.

[4] Brandt EH. The flux line lattice in superconductors. Rep Prog Phys. 1995;58(11):1465.

[5] Dam B, Huijbregtse JM, Klaassen FC, Van der Geest RCF, Doornbos G, Rector JH, Testa AM, Freisem S, Martinez JC, Stäuble-Pümpin B, Griessen R. Origin of high critical currents in $YBa_2Cu_3O_{7-\delta}$ superconducting thin films. Nature. 1999; 399(6735):439.

[6] Huijbregtse JM, Klaassen FC, Szepielow A, Rector JH, Dam B, Griessen R, Kooi BJ, de Th M, Hosson J. Vortex pinning by natural defects in thin films of $YBa_2Cu_3O_{7-\delta}$. Supercond Sci Technol. 2002;15(3):395.

[7] Lu P, Li YQ, Zhao J, Chern CS, Gallois B, Norris P, Kear B, Cosandey F. High density, ultrafine precipitates in $YBa_2Cu_3O_{7-x}$ thin films prepared by plasma-enhanced metalorganic chemical vapordeposition. Appl Phys Lett. 1992;60(10):1265.

[8] Wang H, Serquis A, Maiorov B, Civale L, Jia QX, Arendt PN, Foltyn SR, MacManus-Driscoll JL, Zhang X. Microstructureand transport properties of Y-rich $YBa_2Cu_3O_{7-x}$ thin films. J Appl Phys. 2006;100(5):053904.

[9] Holesinger TG, Maiorov B, Ugurlu O, Civale L, Chen Y, Xiong X, Xie Y, Selvamanickam V. Microstructural and superconducting properties of high current metal–organic chemical vapor deposition $YBa_2Cu_3O_{7-\delta}$ coated conductor wires. Supercond Sci Technol. 2009;22(4):045025.

[10] Chen YM, Selvamanickam V, Zhang YF, Zuev Y, Cantoni C, Specht E, Paranthaman MP, Aytug T, Goyal A, Lee D. Enhanced flux pinning by $BaZrO_3$ and $(Gd, Y)_2O_3$ nano-structures in metal organic chemical vapor deposited GdYBCO high temperature superconductor tapes. Appl Phys Lett. 2009;94(6): 062513.

[11] Macmanus-Driscoll JL, Foltyn SR, Jia QX, Wang H, Serquis A, Civale L, Maiorov B, Hawley ME, Maley MP, Peterson DE. Strongly enhanced current densities in superconducting coated conductors of $YBa_2Cu_3O_{7-x}$+$BaZrO_3$. Nat Mater. 2004;3(7): 439.

[12] Aytug T, Paranthaman M, Specht ED, Zhang Y, Kim K, Zuev YL, Cantoni C, Goyal A, Christem DK, Maroni VA. Enhanced flux pinning in MOCVD-YBCO films through Zr additions: systematic feasibility studies. Supercond Sci Technol. 2010; 23(1):014005.

[13] Jha AK, Khare N, Pinto R. Comparison of flux pinning mechanism in laser ablated YBCO and YBCO:$BaZrO_3$ nanocomposite thin films. J Supercond Nov Magn. 2012;25(2):377.

[14] Selvamanickam V, Chen Y, Shi T, Liu Y, Khatri ND, Liu J, Yao Y, Xiong X, Lei C, Soloveichilk S. Enhanced critical currents in $(Gd, Y)Ba_2Cu_3O_x$ superconducting tapes with high levels of Zr addition. Supercond Sci Technol. 2013;26(3):035006.

[15] Xu AX, Khatri N, Liu YH, Majkic G, Galstyan E, Selvamanickam V, Chen YM, Lei CH, Abraimov D, Hu XB, Jaroszynski J, Larbalestier D. Broad temperature pinning study of 15 mol.% Zr-added (Gd, Y)–Ba–Cu–O MOCVD coated conductors. IEEE Trans Appl Supercond. 2015;25(3):6603105.

[16] Varanasi CV, Burke J, Wang H, Lee JH, Barnes PN. Thick $YBa_2Cu_3O_{7-x}$+$BaSnO_3$ films with enhanced critical current density at high magnetic fields. Appl Phys Lett. 2008;93(9):092501.

[17] Tobita H, Notoh K, Higashikawa K, Inoue M, Kiss T, Kato T, Hirayama T, Yoshizumi M, Izumi T, Shiohara Y. Fabrication of $BaHfO_3$ doped $GdBa_2Cu_3O_{7-\delta}$ coated conductors with the high I_c of 85 A/cm-w under 3 T at liquid nitrogen temperature (77 K). Supercond Sci Technol. 2012;25(6):062002.

[18] Hanisch J, Cai C, Huhne R, Schultz L, Holzapfel B. Formation of nanosized $BaIrO_3$ precipitates and their contribution to flux pinning in Ir-doped $YBa_2Cu_3O_{7-\delta}$ quasi-multilayers. Appl Phys Lett. 2005;86(12):122508.

[19] Harrington SA, Durrell JH, Maiorov B, Wang H, Wimbush SC, Kursumovic A, Lee JH, MacManus-Driscoll JK. Self-assembled, rare earth tantalate pyrochlore nanoparticles for superior flux pinning in $YBa_2Cu_3O_{7-\delta}$ films. Supercond Sci Technol. 2009;22(2):022001.

[20] Wee SH, Goyal A, Specht ED, Cantoni C, Zuev YL, Selvamanickam V, Cook S. Enhanced flux pinning and critical current density via incorporation of self-assembled rare-earth barium tantalate nanocolumns within $YBa_2Cu_3O_{7-\delta}$ films. Phys Rev B. 2010;81(14):140503.

[21] Feldmann DM, Holesinger TG, Maiorov B, Foltyn SR, Coulter JY, Apodaca I. Improved flux pinning in $YBa_2Cu_3O_7$ with nanorods of the double perovskite Ba_2YNbO_6. Supercond Sci Technol. 2010;23(9):095004.

[22] Emergo RLS, Wu JZ, Haugan TJ, Barnes PN. Tuning porosity of vicinal films by insertion of nanoparticles. Appl Phys Lett. 2005; 87(23):232503.

[23] Haugan T, Barnes PN, Wheeler R, Meisenkothen F, Sumption M. Addition of nanoparticle dispersions to enhance flux pinning of the $YBa_2Cu_3O_{7-x}$ superconductor. Nature. 2004;430(7002):867.

[24] Takahashi K, Yamada Y, Konishi M, Watanabe T, Ibi A, Muroga T, Miyata S, Shiohara Y, Kato T, Hirayama T. Magnetic field dependence of J_c for Gd-123 coated conductor on PLD-CeO_2 capped IBAD-GZO substrate tapes. Supercond Sci Technol. 2005;18(8):1118.

[25] Selvamanickam V, Chen Y, Zhang Y, Guevara A, Shi T, Yao Y, Majkic G, Lei C, Galtsyan E, Miller DJ. Effect of rare-earth composition on microstructure and pinning properties of Zr-doped $(Gd, Y)Ba_2Cu_3O_x$ superconducting tapes. Supercond Sci Technol. 2012;25(4):045012.

[26] Xiong J, Xue Y, Xia YD, Zhang F, Zhang YX, Li LH, Zhao XH, Tao BW. Fabrication of long-length ion beam-assisted deposited MgO templates for YBCO-coated conductors. Rare Met. 2013; 32(6):574.

[27] Yang C, He YY, Chu JW, Xue Y, Zhang F, Wang H, Tao BW, Xiong J. Tailoring surface roughness of $LaMnO_3$ buffer layers for YBCO-coated conductors. Rare Met. 2015;34(12):859.

[28] Zhang F, Xiong J, Zhao RP, Xue Y, Wang H, Wang QL, He YY, Zhang P, Tao BW. Temperature-modulated growth of MOCVD-derived $YBa_2Cu_3O_{7-x}$ Films on IBAD-MgO templates. J Supercond Nov Magn. 2015;28(9):2697.

[29] Prado F, Caneiro A, Serquis A. High temperature thermodynamic properties, orthorhombic/tetragonal transition and phase

stability of $GdBa_2Cu_3O_y$ and related R123 compounds. Phys C. 1998;295(3–4):235.

[30] Shi DQ, Ko RK, Song KJ, Chung JK, Choi SJ, Park YM, Shin KC, Yoo SI, Park C. Effects of deposition rate and thickness on the properties of YBCO films deposited by pulsed laser deposition. Supercond Sci Technol. 2004;17(2):S42.

[31] Augieri A, Galluzzi V, Celentano G, Angrisani AA, Mancini A, Rufoloni A, Vannozzi A, Silva E, Pompeo N, Petrisor T, Ciontea L, Gambardella U, Rubanov S. Transport property improvement by means of BZO inclusions in PLD grown YBCO thin films. IEEE Trans Appl Supercond. 2009;19(3):3399.